COOLER EXPERIMENT PREPARATION

COOLER TARGET DEVELOPMENT

1. Overview

F. Sperisen

The Cooler Target Lab's highest priority in the summer of 1989 was to conclude the extensive development work on microparticle targets with a test in the Cooler ring. In a two-shift run in July, 45 and 120 MeV stored, cooled proton beams were scattered from a beam of graphite microparticles of average diameter around 5 μm. The time-averaged target thickness, deduced from the known elastic p-^{12}C cross-section, ranged from $3 \cdot 10^{13}$ to $2 \cdot 10^{15}$ atoms/cm^2. This experiment, demonstrating the feasibility of internal microparticle targets, is described in section 2 below.

In November we reinstalled the gas jet target in the Cooler G-section as the completion of CE-01 (pp $\rightarrow$ ppπ° near the energy threshold) became the primary goal of Cooler activities. In addition to CE-01, the jet target has also been used for CE-08 pp analyzing power in the Coulomb-nuclear interference region) and CE-09 (electron capture for protons on N_2, Ar, and Xe). Throughout the CE-01 production runs the target has been operated with a cooled nozzle, resulting in a significant increase in H_2 jet density (for the same gas load to the ring). Using position-sensitive silicon detectors to detect recoil protons from elastic pp scattering we were able to measure the target gas density distribution along the beam axis. These and other gas jet related developments are presented in section 3.

Two approved Cooler experiments, CE-02 (excitation of intermediate pionic atom states in p-^{13}C elastic scattering) and CE-06 (measurements of nuclear reactions using recoil detection) will require carbon targets which are thin enough for detection of heavy recoils. Carbon microribbons (which have already had some initial tests in the Cooler beam) appear to be the most promising type of target for these experiments. They fulfill the thickness requirement for heavy recoil detection, and relatively simple techniques can be used to expose them to the Cooler beam. Progress on the development of such techniques is reported in section 4.

The carbon skimmer target has continued to play an important role in a number of different experiments. It has been used as polarimeter target for CE-05/15 (Siberian Snake tests), and for detector studies in CE-01, CE-03 (pp $\rightarrow$ pnπ^+ near the energy threshold) and CE-14 [$^3\vec{\mathrm{He}}(\vec{\mathrm{p}},\mathrm{n})3\mathrm{p}$]. In the near future, it will also serve in polarization measurements for CE-08 and CE-16 (Spin-Splitter test). A significant improvement of the skimmer target performance has been achieved with a newly developed linear motion feedthrough positioner, which is described in section 5.

Finally, work has begun on a simple gas storage cell target to be installed in the Cooler T-section. It will be used for preliminary CE-14 tests, as well as to study beam lifetimes with thin targets of various gases in this non-dispersed straight section. A brief description of the cell target design follows in section 6 below.

2. Microparticle Target Test in Cooler

H. Rohdjess, A. Berdoz, H.O. Meyer, J. Doskow, P.V. Pancella, T. Rinckel, and F. Sperisen

Work on microparticle target development has been going on for a number of years at IUCF. Since microparticles were first proposed[1] as internal targets for storage rings, various approaches to exposing them to the ion beam have been pursued.[2-5] In the spring of 1989 we were ready to prove the feasibility of one of these approaches[4,5] with a test in the Cooler ring. Two shifts of beam time were allocated in July. The data from this experiment have since been analyzed and are the subject of a diploma thesis.[6] A paper has been submitted for publication.[7]

The goal of the test in the Cooler ring was to determine the target thickness by measuring a scattering process of known cross-section. For this purpose, the target was installed in the Cooler G-section, utilizing the 1.27 m long general-purpose vacuum chamber and the CE-01 detector,[3,4] which allowed detection of forward scattered protons. Figure 1 shows a top view of the entire setup. A mixture of graphite particles, with a wide range of shapes and sizes (averaging around 5 μm), and nitrogen at atmospheric pressure, is generated in the mixer (see Refs. 4-6 for details). After expansion into vacuum through a 61 cm long stainless steel capillary of 0.41 mm diameter, the dust particles, moving at about 200 m/s, form a beam with a divergence of only about 2^o (half-angle), resulting in a width of 2-3 mm at the interaction point. This fact allows efficient removal of the carrier gas in two differential pumping stages before the target particles intersect with the Cooler beam. The dust beam is then collected in a catcher, consisting of a stack of glass cones with decreasing openings, designed to slow down the particles by multiple impact and to reduce the solid angle for backscattering into the target chamber.[6,7] The catching efficiency is estimated to be well over 99%. The pressure in the target region is maintained at $4.3 \cdot 10^{-7}$ Torr with a 3500 l/s cryo pump (Leybold RPK 3500). Another cryo pump with the same pumping speed is installed on the upstream section of the large box, keeping the vacuum upstream and downstream of the central target region at $2.3 \cdot 10^{-8}$ and $1.0 \cdot 10^{-7}$ Torr, respectively. The target thickness is adjustable by varying the membrane excitation of the mixer. A solenoid-operated shutter at the entrance of the capillary allows for fast gating of the target beam synchronized with the Cooler cycle. Mie-scattering of light from an Argon laser,[3-7] directed onto the dust beam vertically from above (not shown in Fig. 1), is used to monitor the microparticle flux online. In our test, time-averaged thicknesses ranging from $3 \cdot 10^{13}$ to $2 \cdot 10^{15}$ atoms/cm^2 were produced. Larger values (up to 10^{16} atoms/cm^2) are feasible but were not used because the beam lifetime became very short. The mass flow of microparticles necessary for a target thickness of 10^{15} atoms/cm^2 is around 0.13 mg/s.

Cooled beams of 45 and 120 MeV protons were scattered elastically from the carbon microparticles. The CE-01 detector[3,4] was used to detect scattered protons at angles $2^\circ \leq \vartheta_{lab} \leq 11^\circ$. Its ray-tracing capability allowed us to distinguish events originating from background scattering sources. Using 122 MeV elastic p-^{12}C cross-section data,[8] the time-averaged carbon target thickness could be determined with an overall normalization uncertainty of 20%, mainly due to the beam current normalization. Similarly, we have also

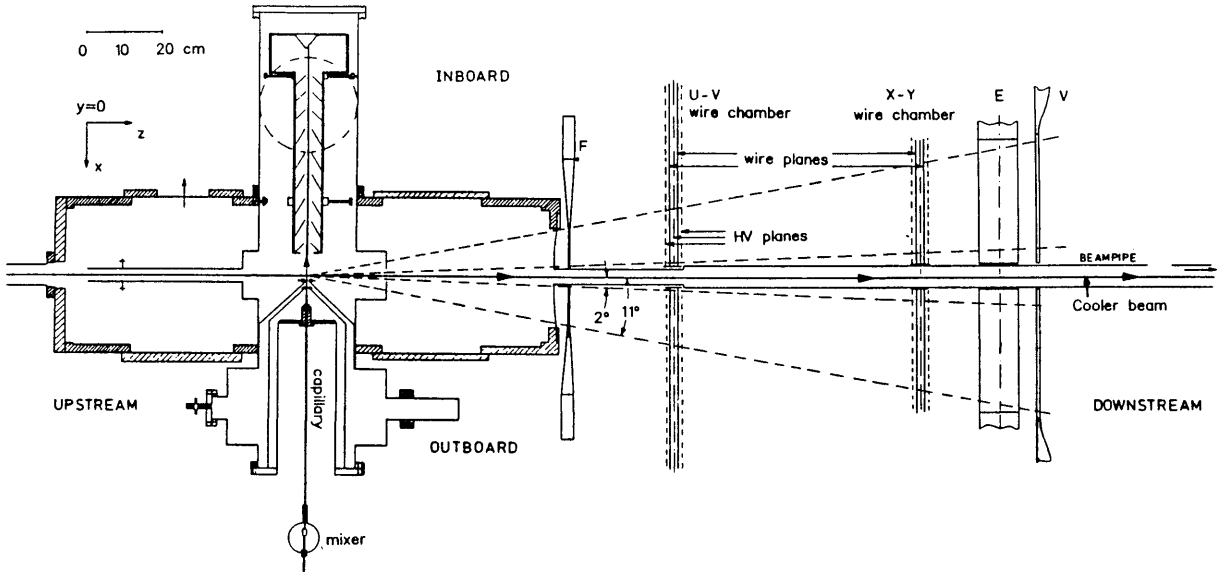

Figure 1. Cross-sectional top view of the microparticle beam target assembly in the target box and the CE-01 detector.

measured the thickness of the N_2 carrier gas alone by turning the mixer off. We obtained $(8.5 \pm 0.9) \cdot 10^{12}$ atoms/cm^2 (about three times more than was calculated based on the ion gauge pressure measurement). This target contamination may be a problem for certain experiments and should be addressed in future development work.

At 120 MeV seven runs with different mixer conditions, i.e. different target thicknesses, were carried out. During a given run, the target thickness varied by as much as a factor of 2, caused by a slow drift of the conditions in the mixer. For this reason, the runs were subdivided into a number of short time intervals. For each interval the target thickness was deduced from proton scattering and the ion beam lifetime was calculated from the time dependence of the recorded signal of the beam intensity monitor. The final result is shown in Fig. 2. It clearly demonstrates that the microparticle beam can provide a target in the desired thickness range, easily variable over two orders of magnitude. Also shown in Fig. 2 are theoretical predictions[9] based on on a model in which the loss of beam ions is driven by Rutherford scattering and the excitation of betatron oscillations by energy loss in the collision of ions with electrons. The material in the target, as well as the residual gas in the remainder of the ring is taken into account. At the time of this test, the technique to measure the Cooler acceptance was not yet in routine use. For this reason, calculations have been carried out for two values of the ring acceptance, in order to show the dependence of the model on this parameter. Any disagreement with the measured lifetime in Fig. 2 probably demonstrates that our current understanding of lifetimes of cooled beams is not yet complete; it should not be used to deduce a value for the ring acceptance, nor should it be interpreted as evidence against the validity of the time-averaging assumption for solid targets.

Our test has established the feasibility of microparticle internal targets. The method should be applicable to a variety of materials. Besides reducing the target contamination

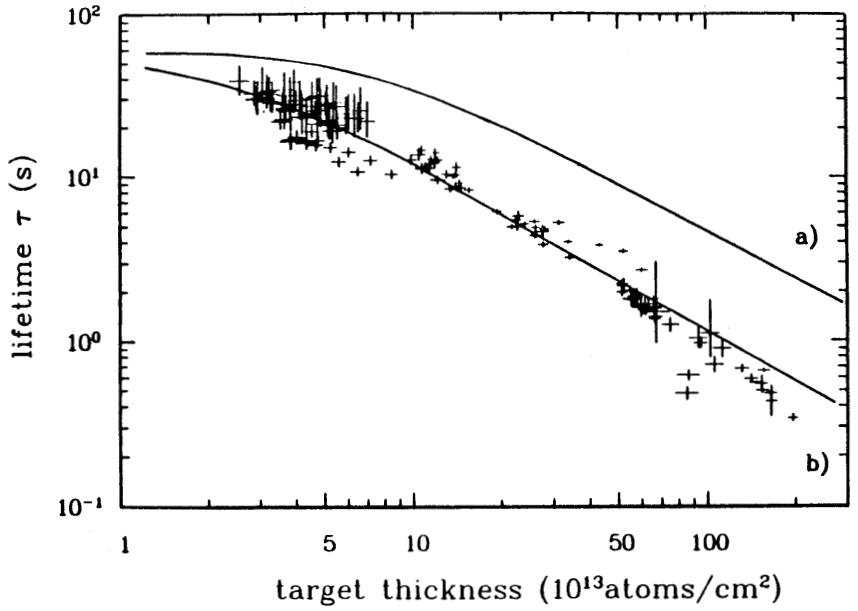

Figure 2. Lifetime of a 120 MeV proton beam as a function of the time averaged thickness of a graphite microparticle target. The target thickness is deduced from the measured elastic scattering rate. The curves shown are preliminary predictions[9] described in the text. Two calculations with an assumed ring acceptance of 9 π mm·mrad (a) and 4 π mm·mrad (b) show the dependence on this parameter. The ring acceptance at the time of this test is not known, nor is it possible to deduce it from this measurement due to uncertainties in the model.

due to the carrier gas, as mentioned above, future development may include continuous feeding of the mixer and improvement of the long-term stability of the particle density. The reason for the finite divergence of the microparticle beam is not well understood: more detailed studies of this are planned in the future.

3. Gas Jet Target

F. Sperisen, J. Doskow, H. Hardner, H.O. Meyer, M.G. Minty, P.V. Pancella, S. Pate, T. Rinckel, A. Ross, and B. von Przewoski

The gas jet target has been operational since March 1988. Over the past year, it has been used mainly for CE-01, initially with the jet located at the center of the 1.27 m long chamber in the G-section. A detailed description of this setup and the basic performance parameters can be found in a previous report.[3] In March 1990 the target was rearranged with the jet in the downstream section of the chamber, as shown in Fig. 3. This change was necessary to obtain the larger acceptance angle of the detector needed to cover the higher energies of CE-01.[10] Following is an update of the major jet-related developments and improvements of the past year.

Although nozzle cooling has been provided in our setup[3] from the beginning, we used it for the first time as we entered the production phase of CE-01 last winter. Lowering the

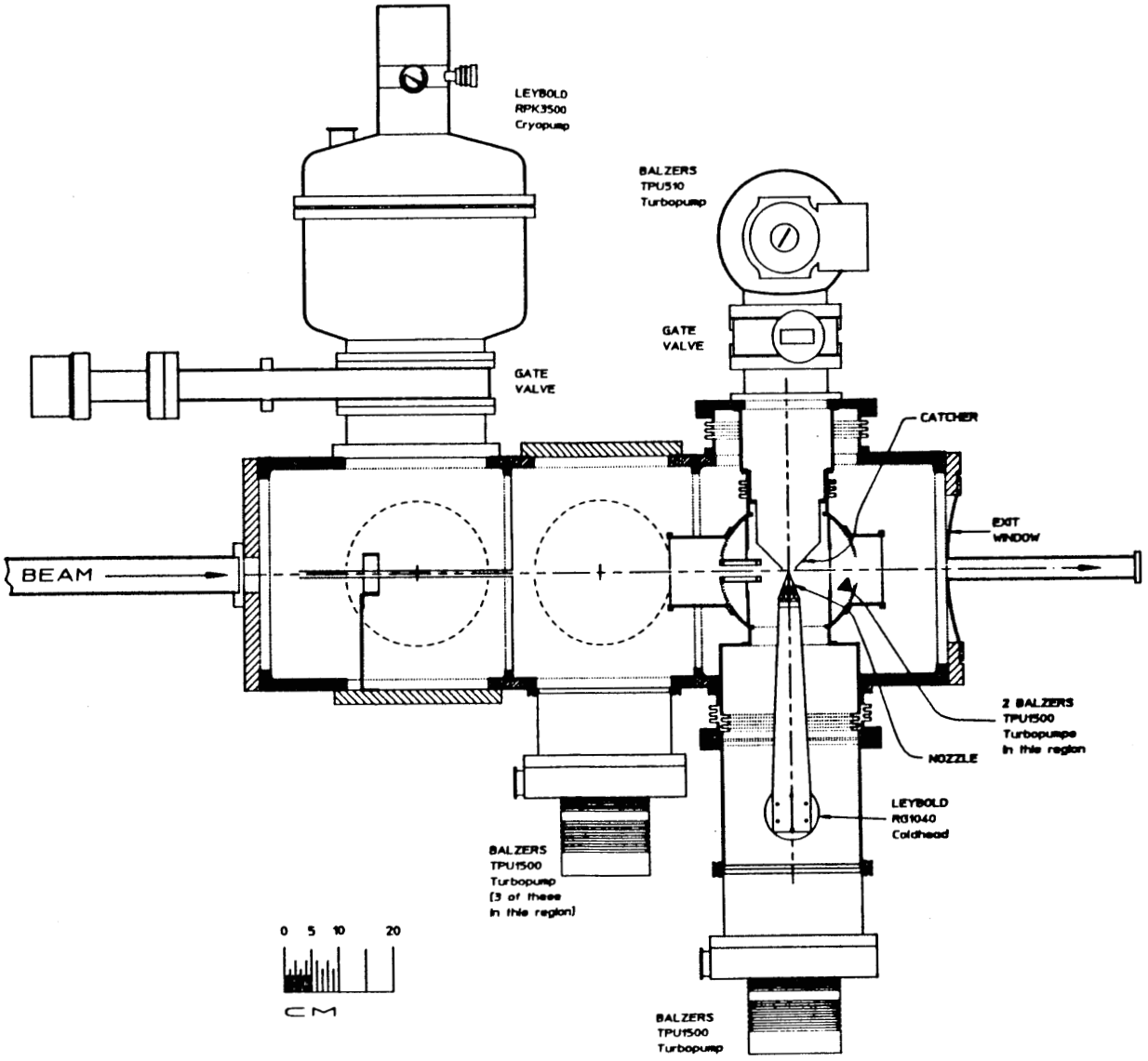

Figure 3. Side view of the jet target setup in the downstream section of the vacuum chamber in the Cooler G-region.

gas temperature increases the jet density proportional to $T^{-1/2}$ at constant gas flow rate, i.e. at constant gas load to the Cooler (we have previously observed[3] that the catching efficiency is not significantly different for warm and cold jets). The nozzle is coupled to the cold head of a closed-cycle helium expander (Leybold RG1040 with RW6 compressor) which has a cooling capacity of about 15 W at 20°K. The temperature is controlled with an electric resistance heater and measured by a platinum resistor (RTD PT-102 by Lake Shore Cryotronics, Inc.), sunk into the nozzle body close to its tip. Independently, we have deduced the gas temperature from measurements of the flow rate vs. pushing pressure, which is a linear function with a slope proportional to $T^{-1/2}$ for an ideal gas. The two

methods agree within a few degrees Kelvin. Typically, during CE-01, the pushing pressure was kept at 100 Torr and the heater power at 14 W. This resulted in a flow rate of 1.65 Torr·l/s (at room temp.) and a temperature of about 40°K. At lower temperatures the nozzle closed up, presumably from condensation of some gas impurity. In an attempt to solve this problem we have installed two purifiers (models 451 and 453 from Matheson Gas Prod., removing oil, water, and particles over 5 μm), improved the efficiency of the LN_2 trap, and replaced all plastic tubes in the gas supply system with copper tubes. This effort, however, has not enabled us to run the jet any colder than before.

The measurement of the π° production cross-section in CE-01 is normalized via the known elastic pp scattering cross-section. The task of monitoring the target thickness by detecting elastic pp scattering is complicated, however, by the fact that a significant fraction of the target gas extends over the differential pumping stages up- and downstream of the jet. Therefore, not just the thickness of the jet itself but also the gas density distribution outside the jet has to be measured. This has been achieved by using position sensitive silicon detectors, installed to the left and right of the jet, detecting recoil protons in coincidence with the corresponding proton going forward into the CE-01 detector. This arrangement also serves to eliminate background scattering originating from apertures, etc., close to the jet. For details see elsewhere in this report.[10] Figure 4 shows an H_2 density distribution around the jet, obtained from vertex reconstruction using the position information of the left recoil detector and the CE-01 wire chambers. The 287 MeV proton beam intercepted the jet about 3 mm above the nozzle, and the pushing pressure was 160 Torr. The curve in Fig. 4 is a fit to the measured background gas density outside the jet ($|z| \geq 1.0$ cm), taking into account the properties of the differential pumping system (see Fig. 3). The total target thickness is $4.7 \cdot 10^{15}$ atoms/cm^2, with the background gas accounting for about 21%. The density normalization is based on a previous measurement using small angle scattering of 25 keV electrons;[11] its uncertainty is estimated to be roughly 30%. Unfortunately, a normalization based on elastic pp scattering of CE-01 suffers from a much larger uncertainty of the beam intensity measurement. (This is not a problem, however, for normalizing the π° production rate in CE-01; it is sufficient to know the integrated *luminosity*, which we expect to determine to within ~5%).

The previously smooth running of the jet target over many hundred hours was interrupted recently by a series of failures of some of our 1500 l/s turbomolecular pumps (Balzers models TPU 1500 and TPH 1500), which provide most of the pumping capacity. These pumps are specified to be run with the rotation axis in any orientation from horizontal to vertical (high vacuum flange up). However, from the nature of the failures (leaking oil into the vacuum chamber, rough running and bearing failure) we concluded that these pumps cannot be run reliably in the horizontal orientation. In fact, Balzers has recently discontinued selling this model, citing problems similar to the ones we have experienced. In order to run all pumps vertically, we have installed three elbows and a cross tube (25 cm diameter) to connect four pumps to the side ports of the vacuum chamber. The reduction in pumping speed amounts to 11% for H_2 and 29% for N_2.

Another modification worth mentioning here concerns the bakeability of the jet target vacuum chamber. Previously, Viton O-rings were used between flat flanges and the knife-edges of the four ports of the chamber section where the jet is located. These O-rings tend

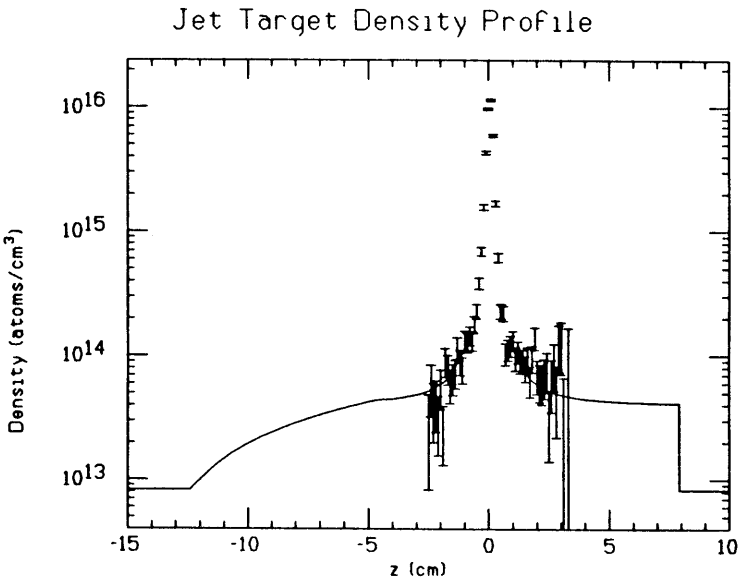

Figure 4. H_2 gas density distribution around the jet, measured by elastic scattering of a 287 MeV proton beam, ~3 mm above the nozzle. The curve represents the background gas density, fitting the measured points outside the jet and taking into account the properties of the differential pumping system.

to leak when they are baked to temperatures above about 70 or 80°C. The flat flanges, two of them welded to the bellows on top and bottom, another to the 25 cm diameter housing assembly (see Fig. 3), have now been replaced by knife-edge flanges so that copper gaskets can be used. There is still a Viton O-ring sealing the downstream exit window, but it is in a standard groove and thus bakeable to at least 150°C.

Finally, as an important diagnostic tool for future jet developments, a method has been developed for measuring jet density profiles. A 1 keV electron beam is used to ionize molecules or atoms of a gas jet. Measuring the ion current as a function of the position of the electron beam, density profiles of N_2 jets have been obtained; calibration is based on published ionization cross-sections.[12] For details see Ref. 13. We are planning to utilize this method in the near future to study jets of monoatomic gases, the width of which is predicted to be only about half that of diatomic jets.

4. Microribbon Targets

First tests with carbon microribbon targets in the Cooler have been reported previously.[4] We found that useful average target thicknesses around 10^{15} atoms/cm^2 can be achieved if the ribbons oscillate across the beam with amplitudes of 5 to 10 mm. Oscillations were excited by an alternating electric field from a single electrode. However, in this simple setup the ribbon motion proved to be unstable at times, especially while moving it in and out of the beam. Precise periodicity is an important feature, particularly if the oscillating microribbon is to be used to scan the ion beam intensity profile. In preparation for two experiments that require detection of heavy recoils from thin carbon

targets, CE-02 and CE-06, work on various methods of microribbon motion has recently been resumed. Following are progress reports on two different approaches.

4.1 Electrically Induced Fiber Oscillation

M.G. Minty, J. Budnick, and W. Lozowski

We have observed periodic oscillations of a thin fiber using the experimental setup depicted in Fig. 5a. By applying 45° phase-shifted sine waves to four electrodes positioned symmetrically about the fiber, one seeks to induce a jumprope-like oscillation of the fiber. A laser beam is directed perpendicular to the fiber. Light diffracted upon intersection of the laser beam with the fiber is detected by a photodiode as shown in Fig. 5b. By moving the laser beam across the fiber, the time interval between successive light bursts may be measured as a function of the laser position. An oscilloscope display of a typical

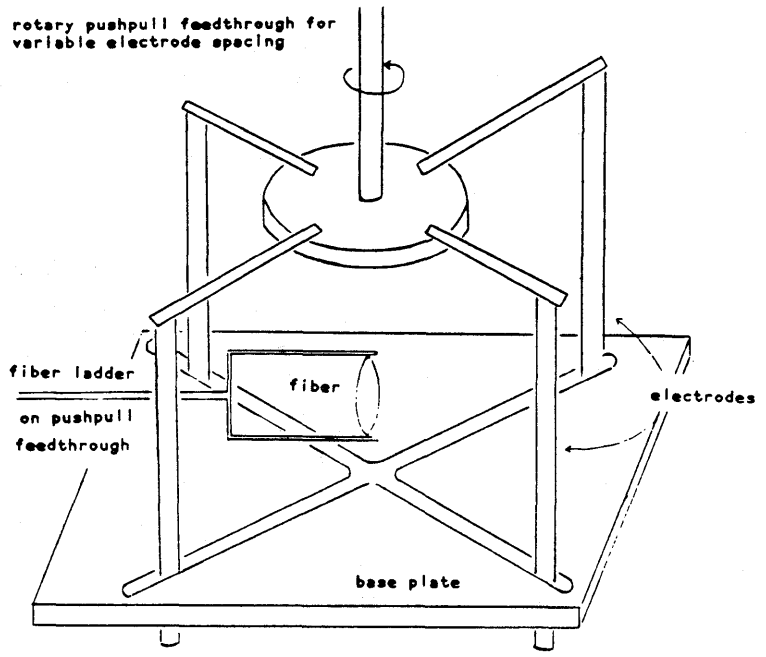

Figure 5a

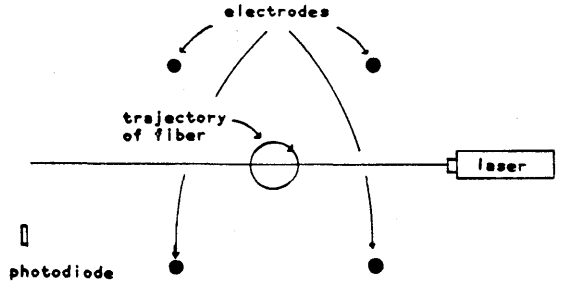

Figure 5b

Figure 5. Experimental setup for electrically induced fiber oscillations; (a) perspective view; (b) top view.

Figure 6. Typical output from photodiode - laser monitor. The photodiode signal (upper trace, 500 mV per division) due to light diffracted off the fiber when triggered on the driving alternating voltage (lower trace, 1 V per division, before amplification). The time scale is 5 ms per division.

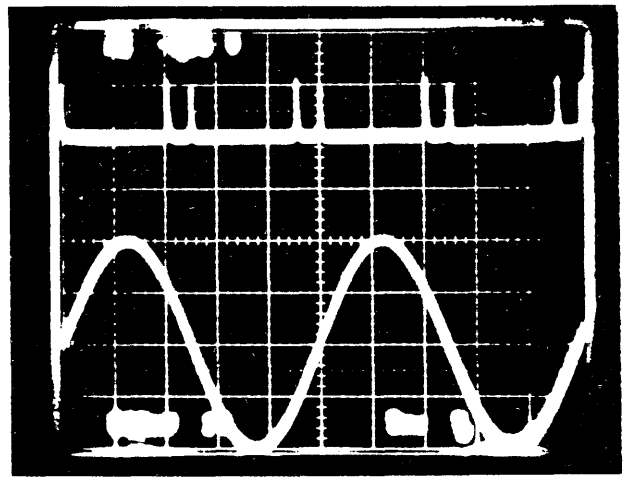

measurement is presented in Fig. 6, which depicts the photodiode signal (upper trace) when triggered on one of the four sinusoidal voltages (lower trace). Associated with each period of the sine wave are four light bursts. Two bursts result from the fact that the force experienced by the fiber depends only on the magnitude of the applied field; i.e. the revolution frequency of the fiber is twice the driving frequency. The other two bursts correspond to two laser-fiber intersections per revolution of the fiber. The results of a trajectory scan are given in Fig. 7, where the time interval between successive light bursts is plotted as a function of the laser position. In this case a 6.5 μm C fiber was used with an 80 Hz revolution frequency. The electrode peak to peak voltage amplitude was 775 V and spacing between adjacent electrodes was 8.6 cm. The error bars reflect the uncertainty in measuring the time interval on the oscilloscope display. The expected time interval

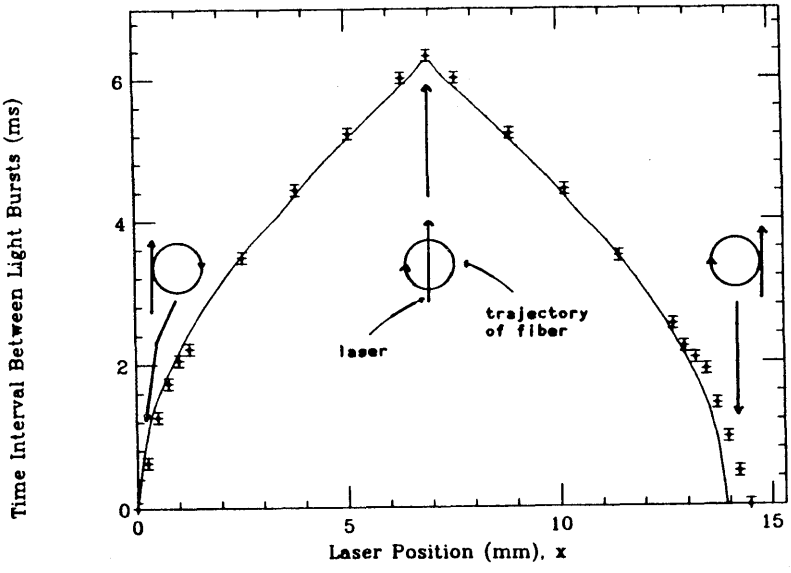

Figure 7. Measured and calculated time intervals between subsequent fiber passages through the laser beam as a function of the laser position.

between successive light bursts may also be calculated. Assuming that the midpoint of the fiber moves on a circular trajectory at constant velocity one finds the following relation:

$$\Delta t = \frac{1}{2\pi f_o} sin^{-1} \sqrt{1 - \left(\frac{x-r}{r}\right)^2},$$

where f_o is the driving frequency, r is the measured trajectory radius (7.0 mm), x is the position of the laser as show in Fig. 7, and Δt is the time between the two closest light bursts.

The calculated curve is in good agreement with the data which indicates that the fiber motion is indeed uniform in the transverse plane. Observations made with a strobe light tuned to the fundamental frequency of revolution showed that there were no higher order excitations. By expanding the time scale on the oscilloscope and measuring the jitter in photodiode peak position, the position resolution was found to have an upper limit of 0.52 mm. The oscillating fiber described above would present an average thickness of $1.7 \cdot 10^{16}$ atoms/cm^2 to the Cooler beam. In order to attain thinner targets on the order of 10^{15} atoms/cm^2, we will repeat these studies using microribbons.

4.2 Mechanical Fiber Oscillation

P.V. Pancella, J. Doskow, and W. Lozowski

We have recently proven in principle another method for presenting a fiber target to the Cooler beam. This was simply one or more microribbons each with one end attached to a spinning disk, the other end hanging free. Resembling a popular type of lawn trimmer (Fig. 8), the centrifugal force stretches the ribbon(s) straight, producing a time-averaged target in the shape of a disk.

In the test setup, a variable-speed electric motor was coupled directly to the shaft of a Ferro-fluidic feed-through, a device for transfering high-speed (up to 30,000 rpm) rotational motion into high vacuum. An aluminum spindle ending in a 2 cm diameter disk was mounted to the vacuum side of the feed-through, and two microribbons were glued at opposing points to the circumference of the disk. Each ribbon was about 2.5 cm long, 100 μm wide and 20 μg/cm^2 thick. A smooth, insulating sleeve covered most of the aluminum spindle. Before the rotation started, the ribbons adhered lightly to this sleeve, apparently by an electrostatic force. As before, the glue used to attach the ribbons allows a conducting path between the ribbon and the spindle at ground potential. These ribbons survived several start/stop cycles without tangling or breaking, and rotational speeds up to 150 Hz, limited by the power of the motor.

For given ribbon dimensions (linear density) the average target thickness seen by a beam almost parallel to the rotation axis varies inversely with the distance from that axis. If two ribbons are mounted, the thickness is calculated as in the case of the "jump-rope" configuration,[4] with the amplitude of the fiber oscillation replaced by the radius to the beam intersection point. In practice, this radius can be adjusted down to the radius of the supporting disk, allowing the possibility of some target thickness adjustment by moving the beam. In this test the ribbons had roughly ten times the linear density as the thinnest

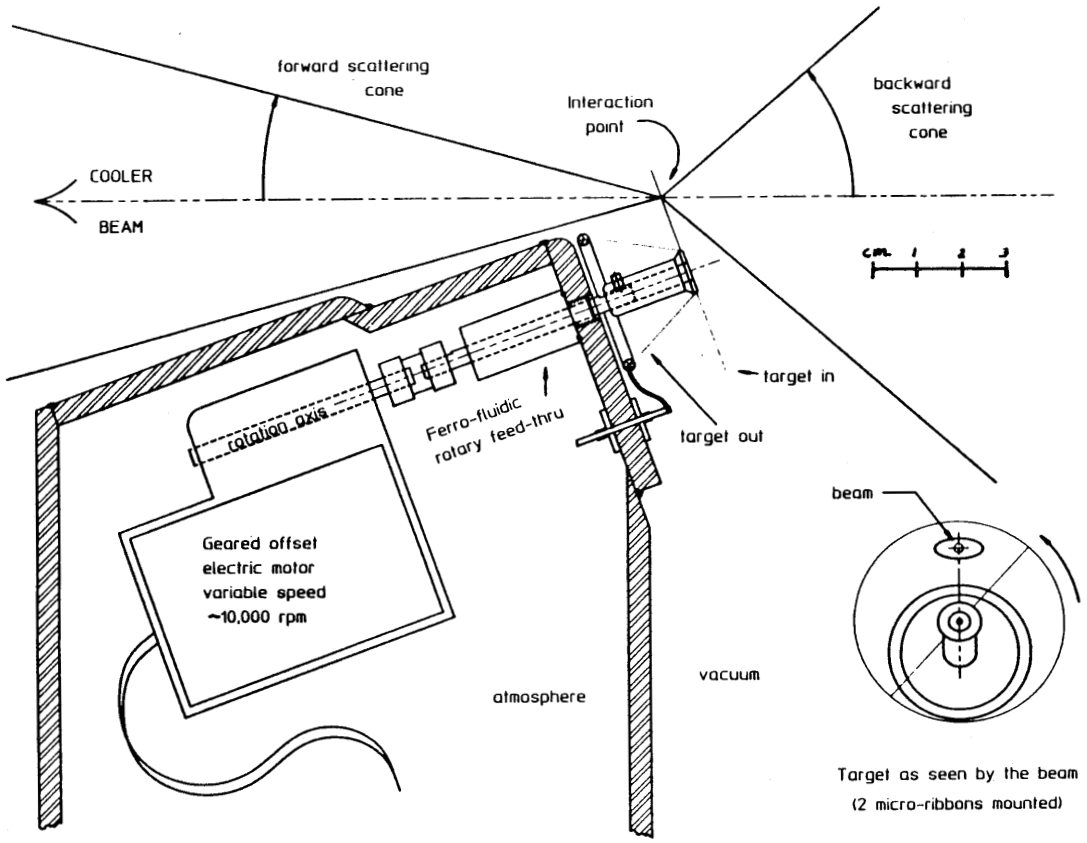

Figure 8. A possible configuration for a spinning fiber target in a chamber like the "G" target box in the Cooler, approximately to scale. The clear scattering angles shown are for CE-02.

ones used in previous tests in the Cooler beam,[4] but the effective radius is roughly five times larger, resulting in $\sim 10^{15}$ atoms/cm^2, i.e. about twice the average target thickness as for previous tests. Thinner ribbons can provide a thinner target, but are more difficult to handle.

This greater effective amplitude, along with the 150 Hz revolution frequency, yields a fiber speed at the beam which is about 10 times greater than it was during the in-beam tests reported last year.[4] This is significant if the transit time of each beam passage must be reduced to decrease the likely number of events per passage. Calculations show that the ribbons should survive even higher speeds, thus with multiple ribbons it should be possible to approach 1000 passages per second, and ribbon speeds of 5000 cm/s at the beam location.

The duty factor in this method ($\sim 10^{-3}$) can only be increased (for the same average target thickness) by using thinner ribbons and more of them, or a smaller radius. If thinner ribbons are required, we will have to study better methods to handle them on installation and start/stop. One possibility, shown in Fig. 8, would be a stationary charged ring which would attract the ribbons. This might also serve to move the target in and out of the beam even while the disk is still spinning.

We are now in the process of identifying a reliable electric motor to use for further tests. The device could be configured as shown (Fig. 8) for use in the Cooler. A vacuum chamber would mount to the top, bottom, or side of the G-box, for instance. Forward and backward scattered particles could be cleanly detected up to some angle as shown. We assume that the ribbons would be out of the beam when rotation is stopped, and that the first passage on startup would be sufficiently fast so as not to destroy the stored beam. Alternatively, some electrostatic manipulation may be required to cycle the target in and out with the Cooler fill cycle without stopping the high-speed rotation every cycle, as mentioned above. It would be possible but less desirable to mount the entire device on a bellows and move the entire assembly in and out of the beam, again with ribbons rotating continuously.

5. Linear Motion Feedthrough for Target Positioning

P.V. Pancella, T. Sloan, J. Frey, D. Duncan, and J. Graham

A device for providing controlled linear motion in very high vacuum has been developed for manipulating targets in the Cooler. It was designed for speed, precision, and long lifetime in constant operation. No bellows or sliding vacuum seals are employed. Total linear travel is 20 cm, and the maximum *controlled* speed so far observed is about 15 cm/s, but this may be increased. The actuator should function in any orientation. Two units have been built, but controls are still in development. Initial testing has been successful. Although it is expected that these new actuators will be more reliable than the rotary devices they are meant to replace, they have yet to be tested in operation over long periods of time.

The linear actuator itself is very simple. It is a copy of a device built and used on the AGS at Brookhaven National Laboratory[14] which uses standard linear motor and position sensing technology. Inside the cylindrical vacuum enclosure, the moving shaft is supported by two linear ball bearings and has a samarium cobalt permanent magnet rigidly attached to it. (Fig. 9) Outside the vacuum, a pair of driving coils cause the shaft to move by electromagnetic coupling to the permanent magnet through the stainless steel vacuum enclosure. An extension of the shaft contains a ferromagnetic "core" whose position can be sensed by the coils of a linear variable differential transformer (LVDT). The output of the LVDT is an analog signal (± 10 Volts) so that the position resolution is limited only by electronic noise.

The tube containing the shaft is welded to a 6-inch knife-edge flange and is completely sealed. The driving coils and LVDT pickup are outside the vacuum. Everything in vacuum is made of stainless steel or samarium cobalt, except for the Delrin housing of one of the bearings. The device is bakeable to 150°C or so, and is compatible with vacuum in the low nanotorr range. The bearings are dry lubricated with Molybdenum disulfide powder, and there is very little outgassing after a brief bakeout.

The control circuit incorporates a standard feedback loop which compares the desired position with the readout of the LVDT. So far, the commercial software development package being used permits only simple movements on command, with control of speed, acceleration, and other parameters of the feedback circuit. We are in the process of providing interrupt capability and additional software which will allow programmed movements

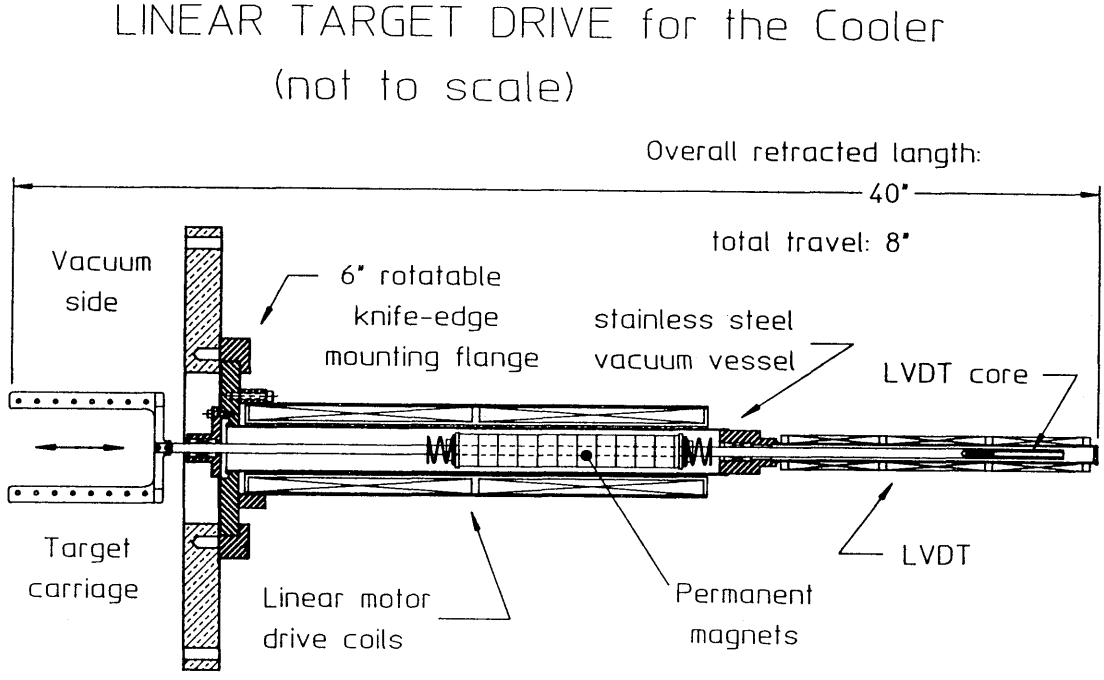

Figure 9. Cutaway view of the Linear Actuator, shown in retracted position with an empty target carriage. The horizontal scale has been compressed relative to the vertical.

to be synchronized with the Cooler fill cycle or other triggering events. The present user interface is through an IBM personal computer.

The primary use for this device is to present solid targets to the Cooler beam, particularly in the "skimmer" target mode.[4] Such a target is useful for Cooler polarimetry, and one of these motors was already used in the March CE-15 Siberian Snake run.[15] Skimmer targets are also useful for energy calibration and tracking checkout of the CE-01 detector stack, as they provide the most localized scattering source yet seen in the Cooler. The precise positioning capability can also be used to locate the beam or to calibrate nearby BPM's. A second unit was installed in the I-region to help locate the injected beam path relative to the closed orbit.

Future uses include a moveable mount for fiber targets, and possibly a beam profile measurement. If sufficient speed can be achieved with precise position readout, then one can measure the current loss caused by quickly intercepting part of the beam at a known location. The loss measured by the BPM system or one of the wall gap monitors as a function of the intercepting position can give beam profile information on a scale of 0.2 mm.

We plan to procede with bench testing in conjunction with software controls development to determine the limits on speed and precision, and to explore how performance varies with load and orientation. Two complete systems have been built, and controls will be able to operate them independently or in conjunction from the same IBM-PC. It is hoped that these devices will be available for general use in the near future.

6. A Gas Storage Cell Target for the Cooler T-Section

F. Sperisen, J. Doskow, A. Smith, and J. Sowinski

Preparations for the first Cooler experiment with an internal polarized target (CE-14) are underway in the T-section. In this experiment neutrons from the reaction $^3\vec{\text{He}}(\vec{\text{p}},\text{n})3\text{p}$ will be detected around zero degrees. For preliminary studies we have designed a simple storage cell target that should allow us to investigate all experimental aspects not related to target polarization.

The cell consists of a 73 cm long copper tube, with an inner diameter of 3.01 cm. The gas is fed into the tube at the midpoint. We plan to use a gas flow control system, similar to the one of the jet target,[3] which allows turning on and off the gas synchronously with the Cooler cycle, and also varying its flow rate and thus the target thickness. The cell will be mounted in a 116 cm long vacuum chamber, similar to the one used for the jet target. Last November, this chamber, the so called "T-box", has been installed in the T-section, just upstream of the two 3° magnets. Two differential pumping stages will decouple the storage cell from the rest of the ring. The first stage, comprising the cell, will be pumped on by two 1500 l/s turbos (Balzers TPU 1500), mounted on the T-box middle and downstream sections from below. A 10 cm tube restricts the gas flow into the second stage upstream where a cryo pump (Leybold RPK 3500, 1500 l/s for He, 4500 l/s for H_2) will maintain the required ring vacuum of 10^{-9} Torr (N_2 equivalent). To evacuate the second stage on downstream side another cryo pump (same model) has been installed downstream of the 3° magnets.

The four pumps needed in this setup are not part of the jet target, i.e. both targets can be installed at the same time. Even with the limited pumping capacity available, we can expect target thicknesses close to those expected for the $^3\vec{\text{He}}$-target. The maximum allowed flow rate, $\dot{n}$, through the cell, to not exceed the required ring vacuum, is $7 \cdot 10^{16}$ He atoms/s, about half the expected production rate of $^3\vec{\text{He}}$. This determines the maximum target thickness, which (in atoms/cm^2) is given approximately by

$$t \approx 3.3 \cdot 10^{-5} \sqrt{\frac{M}{T}} \frac{\dot{n}\ell^2}{d^3},$$

where M is the molecular weight (in g/mol), T is the temperature (in °K), ℓ is the length and d is the diameter of the tube (both in cm). For the cell dimensions given above, t = $5.3 \cdot 10^{13}$ He atoms/cm^2 at room temperature. We are planning to cool the cell with a He expander cryo-system that we have received on loan from the University of Alberta. Cooling to 40°K would increase the thickness by a factor of 2.7. To determine the target thickness, we will measure the flow rate, the pressure at the midpoint of the tube, and the temperature along the tube. We are planning to install this target in the summer of 1990.

1. H.O. Meyer, Proc. Workshop on Nuclear Physics with Stored, Cooled Beams, eds. P. Schwandt and H.O. Meyer, AIP Proc. **128**, 76 (1985).
2. IUCF Scientific and Technical Report, 1986.
3. IUCF Scientific and Technical Report, January 1987 - April 1988.
4. IUCF Scientific and Technical Report, May 1988 - April 1989.

5. A. Berdoz *et al.*, Nucl. Instr. Meth. **B40/41**, 455 (1989).
6. H. Rohdjess, *The Parameters of a Microparticle Beam Target and its Test in the Indiana Cooler Ring*, Diploma thesis, University of Hamburg, 1990.
7. H.O. Meyer *et al.*, submitted to Nucl. Instr. Meth. A.
8. H.O. Meyer *et al.*, Phys. Rev. **C27**, 459 (1983).
9. R.E. Pollock, private communication.
10. A. Ross *et al.*, Measurement of the Total Cross Section for the Reaction p+p→p+p+π°, this report
11. F. Sperisen *et al.*, Nucl. Instr. Meth. **A274**, 604 (1989).
12. L.J. Kiefer and G.H. Dunn, Rev. Mod. Phys. **38**, 1 (1966).
13. H. Hardner and F. Sperisen, IUCF Newsletter **45**, 26 (1989).
14. E.R. Beadle, E.S. Rodger, R.E. Thern, *A Beam Scraper Using a Linear Motor*, Brookhaven National Lab internal report BNL-41825, 1989.
15. A.D. Krisch, *et al.*, Overcoming Intrinsic and Synchrotron Depolarizing Resonances with a Siberian Snake, this report.

DETECTOR DEVELOPMENT FOR THE pp→pnπ^+ EXPERIMENT (CE03)

W. Daehnick, S. Dytman, W. Brooks, P.C. Li, J. Hardie,
S. Saha, D. Kreithen, B. Beatty, and Hong Li

• Introduction

The kinematically complete determination of the three-body final state of the p + p → p + n + π^+ reaction requires the measurement of five degrees of freedom of the outgoing particles. The five quantities which may be measured most accurately are the outgoing angles of both nucleons and the energy of the proton. This will be accomplished at the T-site of the Cooler, where a specially-constructed magnet will serve to separate the incident beam from the reaction nucleons and pions. The reaction neutrons will emerge from the target in a narrow cone near threshold and be detected in a neutron hodoscope 3-7 meters (depending on the beam energy) downstream, while the reaction protons will be bent out of the projectile beam and will be detected by two wire chambers and a ΔE-E scintillator assembly. At this time, the neutron hodoscope has been completed, as has one of the wire chambers and a portion of the ΔE-E assembly. These components have been tested in the Cooler beam; a partial offline analysis will be discussed here.

• Neutron Hodoscope

The neutron hodoscope consists of fourteen bars of BC 408 plastic scintillator fitted with fast phototubes at each end. When a scintillation event occurs in a given bar, the time difference between the arrival of the signals at the phototube gives the position of the scintillation along the bar while the position in the perpendicular direction is given by noting which bar fired. Timing and energy calibrations are obtained from pulses fanned